ANALYTIC AND EXPERIMENTAL STUDIES OF NORMAL INLETS, WITH SPECIAL REFERENCE TO FAN-IN-WING VTOL POWERPLANTS

U. W. SCHAUB
Assistant Research Officer

E. P. COCKSHUTT
Senior Research Officer

National Research Council
Ottawa, Canada

PART A. ANALYTIC INVESTIGATION

ABSTRACT

The flow of air into a normal inlet is examined with a simple mathematical model—viz., potential flow into a quasi-circular two-dimensional bellmouth. Streamline maps and surface velocities are presented for various bellmouth radii and cross-flow ratios, using conformal transformation methods. It is demonstrated that the wall contour generated by this method has some deficiencies, but that these are localized and do not affect the flow field as a whole.

Description of a complementary experimental programme is reserved for Part B of this paper.

INTRODUCTION

Several powerplant arrangements for vertically rising (VTOL) aircraft involve the possibility of engine inlets operating perpendicular or normal to the flight vector. The problem is particularly acute when lifting fans are immersed in the plane of a wing, where depth is at a premium. One of

the problems foreseen with a normal inlet is the nonuniform velocit profile which is produced by it; this results in a cyclical loading variatic of the fan rotor blades, which is undesirable from both mechanical ar aerodynamic considerations. A second problem with a normal inlet lies the possibility of flow separation, resulting from unfavourable pressu gradients, further distorting the velocity profile.

The purpose of the present study is hence to examine the severity of tl inlet problem, and to identify the critically important areas.

MATHEMATICAL METHOD

The potential flow solution is obtained through the use of the comple variable conformal mapping technique. A one-to-one correspondence established between the region of interest and a simpler region by means a Schwarz-Christoffel transformation. This function maps the upp half ζ-plane into a sharp-cornered passage as shown below.

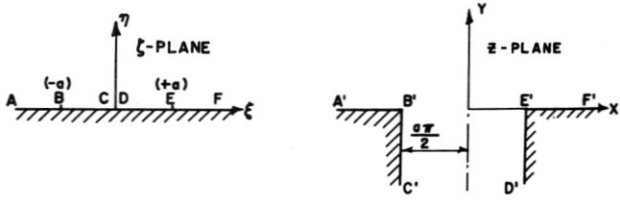

The solution to the flow problem is established in the ζ-half plane and then transferred back to the region of interest, the z-plane.

The mapping function is:

$$z_a = \int \frac{\sqrt{\zeta^2 - a^2}}{\zeta} d\zeta$$

$$= \sqrt{\zeta^2 - a^2} - a \cos^{-1}\left(\frac{a}{\zeta}\right) + \frac{a\pi}{2} \qquad (1$$

where z and ζ are both complex.

A second transformation of the same type may be generated by replacing constant a by a second constant b, and multiplying by a third constant c:

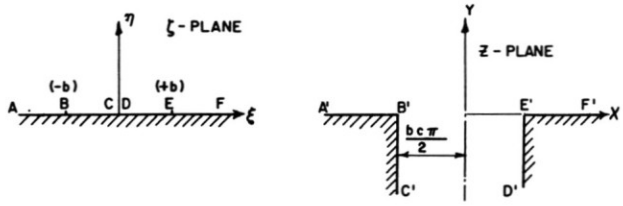

$$z_b = c\left[\sqrt{\zeta^2 - b^2} - b\cos^{-1}\left(\frac{d}{\zeta}\right) + \frac{b\pi}{2}\right] \tag{2}$$

These two transformations may now be added together, yielding the following:

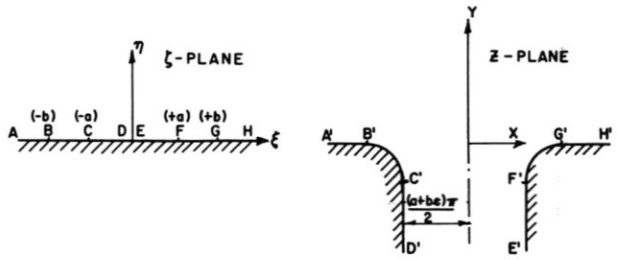

$$z = z_a + z_b \tag{3}$$

It is seen that this dual transformation has replaced the sharp corners by curved contours; it remains to be demonstrated that the contour generated is a useful one.

Two elementary flow patterns are of interest in the ζ-plane—a point sink and uniform parallel flow.

The point sink is described by a potential function:

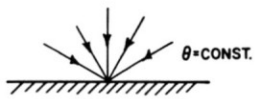

$$F = -M \log \zeta$$

Uniform parallel flow is described by a second potential function:

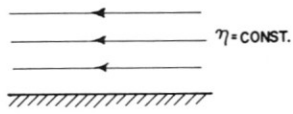

$$F = -N\zeta$$

The combined flow system is then established by superposition:

$$F = -N\zeta - M \log \zeta \tag{4}$$

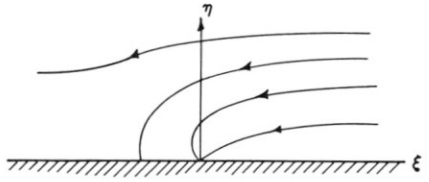

The equations of the streamlines are defined by the stream function, which is the imaginary portion of the potential function, viz.,

$$\psi = -N_\eta - M\theta \tag{5}$$

One of the significant aspects of conformal mapping is that streamlines in the ζ-plane map into corresponding streamlines in the z-plane; hence the transformation generated above may be used to establish the streamlines for combined flow into a contoured inlet.

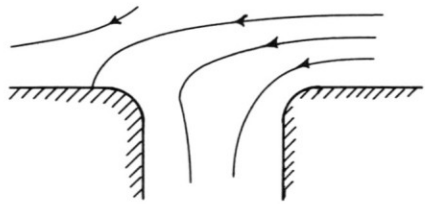

Another feature of conformal mapping is that the conjugate of the velocity is given by the derivative of the potential function:

$$\overline{V(\zeta)} = \frac{dF}{d\zeta} = -N - \frac{M}{\zeta} \tag{6}$$

The corresponding velocities in the z-plane follow similarly:

$$\overline{V(z)} = \frac{dF}{dz} = \frac{dF}{d\zeta}\frac{d\zeta}{dz} = \left(-N - \frac{M}{\zeta}\right)\frac{\zeta}{\sqrt{\zeta^2 - a^2} + c\sqrt{\zeta^2 - b^2}} \tag{7}$$

The method outlined above is indirect, in that one first specifies the coordinates of a point in the ζ-plane, and then finds the coordinates of the image point in the z-plane [Eq. (3)], and the corresponding velocity in the z-plane [Eq. (7)]. The algebraic complexity of the relation between ζ and z makes difficult an explicit solution in the z-plane.

BELLMOUTH CONTOUR

SPECIFICATION OF CONSTANTS

The mapping transformation derived above [Eq. (3)] contained three unspecified constants, a, b, and c. For streamline mapping, the size of the resulting figure is immaterial, and hence one constant may be arbitrarily specified; this is done by setting $a = 1$ (b is assumed greater than a). The coordinates in the z-plane were actually scaled to yield a semiwidth of the inlet passage of unity, so that the transformation became

$$z = \frac{2}{(1 + bc)\pi}[z_a + z_b] \tag{8}$$

In order to secure a general approximation to a circular contour, further constraint was introduced (see sketch below) by requiri $O'B'/O'C' = 1$. (Pseudo-elliptical contours could of course be generated selecting values of this ratio other than unity.)

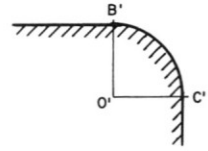

This geometrical constraint produced the following specification foı in terms of b:

$$c = \frac{\pi - \cos^{-1}\left(-\frac{1}{b}\right) - \sqrt{b^2 - 1}}{\sqrt{b^2 - 1} + b \log\left(b - \sqrt{b^2 - 1}\right)} \qquad (1$$

One is further able to specify the radius ratio

$$\frac{R}{D} = \frac{O'C'}{C'F'}$$

$$= -\frac{\sqrt{b^2 - 1} + b \log\left(b - \sqrt{b^2 - 1}\right)}{\pi(1 + bc)} \qquad (1$$

It is clear, therefore, that there is only a single geometrical variable and that this is equivalent to specifying a radius ratio R/D.

COMPARISON WITH CIRCULAR CONTOUR

In Fig. 1*a*, the curve produced by the conformal transformation is coı pared with a circular arc, and in Fig. 1*b*, comparable slope data are pı sented. A radius ratio R/D of 1/8 has been selected for this comparison being reasonably typical—the discrepancy between the generated conto and a circle is reduced as the radius ratio increases towards unity. It seen that, for the radius ratio of 1/8, there is a maximum distance betwe the two contours of about 8 per cent of the circular radius.

Rather more significant are the slope data of Fig. 1*b*, where the abscissa is the longitudinal distance into the bellmouth. While both contours reach the end of the curved portion with zero slope, the circular arc approaches with an approximately constant second derivative (reciprocal of radius of curvature), while the generated contour approaches with an ever-increasing second derivative. From considerations of boundary layer development, an ideal contour for a bellmouth would be characterized by continuity of the *second* derivative through the point of tangency, not just the first derivative, and neither the generated contour nor the circular arc possesses this feature.

STREAMLINE PATTERNS

The results of a systematic variation of the significant flow parameters are contained in a composite figure (Fig. 2). The transformation given above [Eq. (8)] was coded in Fortran II for a 1620 computer; as was described above, the solution was indirect in that streamlines in the ζ-η

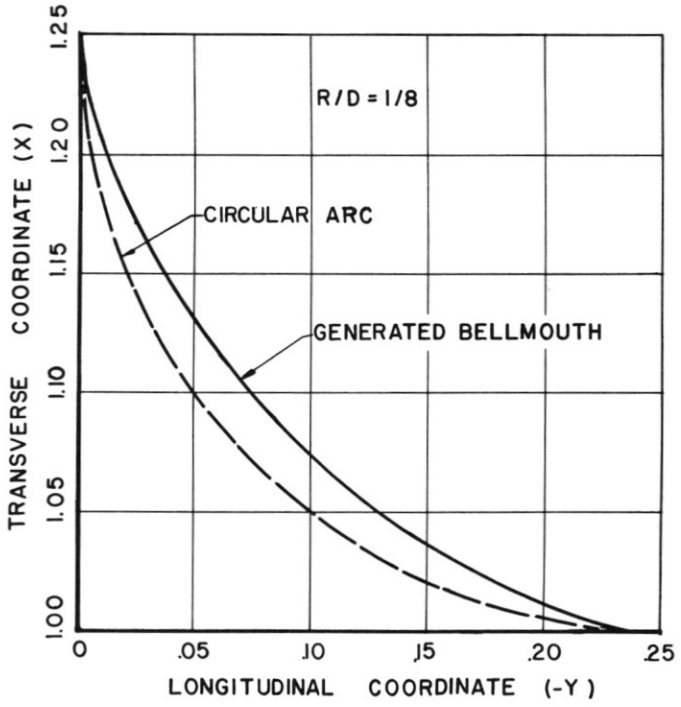

Figure 1*a*. Wall contour profile comparison.

plane were mapped, point by point, into the X-Y plane, the control of point spacing being established by card inputs inserted by the operator. Streamline spacing was established by dividing the streamtube into the inlet into ten equal elements.

Streamline plots are shown in Fig. 2 for 6 values of the radius ratio (lip radius/passage width), viz., 0, 1/32, 1/16, 1/8, 1/4 and 1/2, and for 5 values of the cross-flow ratio (transverse velocity/inlet velocity), viz., 0, 1/4, 1/2, 1, and ∞. The strongest variable influencing the flow pattern is undoubtedly the cross-flow ratio, which may be seen by following across the page the patterns with the square inlet ($R/D = 0$). The stagnation streamline moves closer and closer to the inlet, and at a cross-flow ratio of unity, impinges right on the corner. At the same time, the asymmetry of the inflow increases, with higher and higher velocities near the leading lip, and lower and lower velocities near the trailing lip.

The effects of inlet geometry variation tend to be confined to the immediate area of the inlet, and hence the general appearance of the flow fields is similar as one follows down the series of radius ratios at a constant

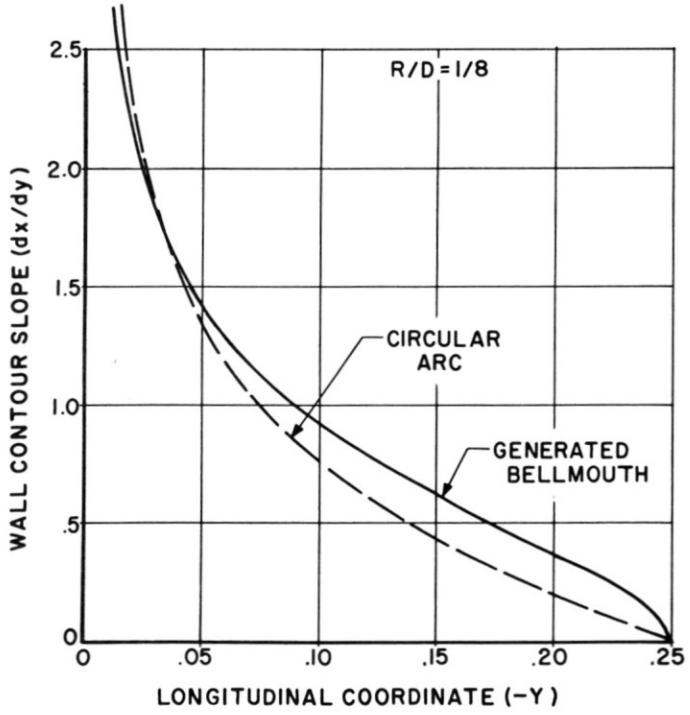

Figure 1*b*. Wall contour slope comparison.

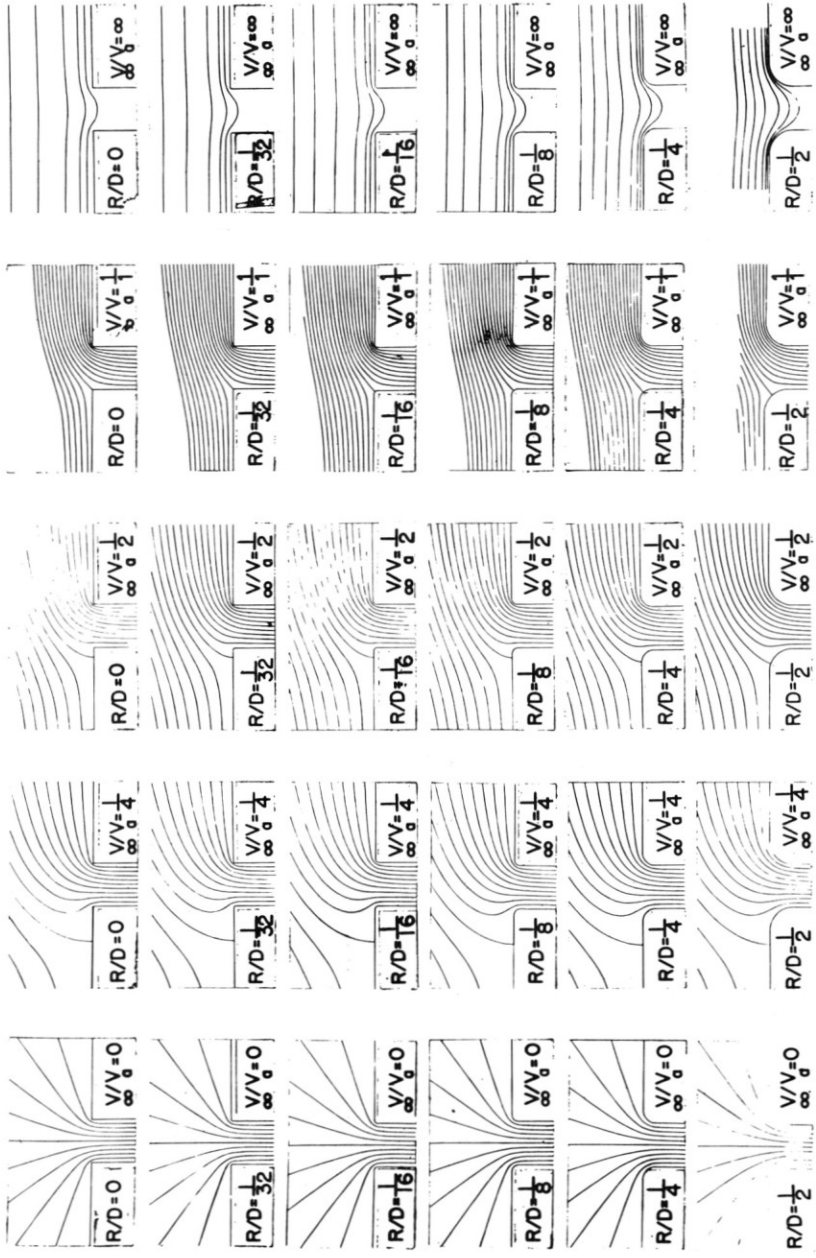

Figure 2. Streamline patterns.

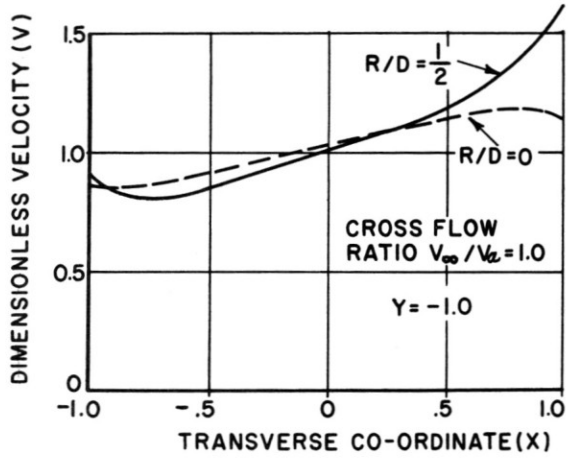

Figure 3. Velocity profile comparison.

cross-flow ratio. Local velocities at the inlet, as evidenced by streamlin spacing, are naturally greatly influenced by the radius ratio, and th merits of keeping the radius large are clear. A slightly less obvious point i that, under cross-flow conditions, depth into the inlet is the prime variabl in achieving uniformity of the flow, not the radius ratio. In fact, a generou radius ratio produces a less uniform velocity profile than a sharp-cornere inlet, at a given distance down the inlet, as is shown in Fig. 3. These con clusions of course are valid only within the limitations of potential flow and would not necessarily apply to real, viscous flow.

SURFACE VELOCITIES

EFFECTS OF RADIUS RATIO AND CROSS-FLOW RATIO

In considering the relative merits of various inlets under static an cross-flow conditions, it is profitable to examine the velocities on th surface of the inlets. It is important to identify local velocity peaks an deceleration rates since these may cause the boundary layer to separate In the various portions of Fig. 4 the bellmouth surfaces are unwrapped o developed to yield a distance parameter as the abscissa, against which th velocity is plotted.

Looking, for example, at the surface velocity distribution for a radiu ratio of 1/8 and zero cross flow, one sees a rapidly accelerating flow up t the start of the bellmouth curvature, a period of steadily increasing velocity

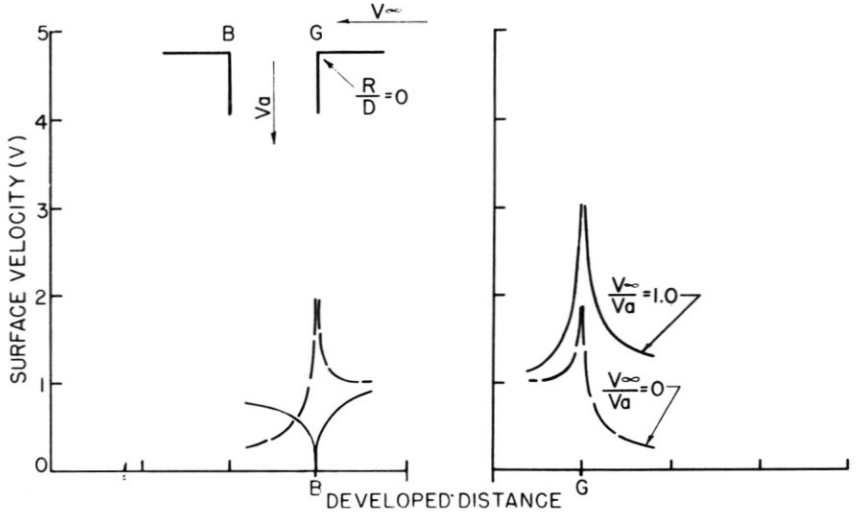

Figure 4*a*. Surface velocities ($R/D = 0$).

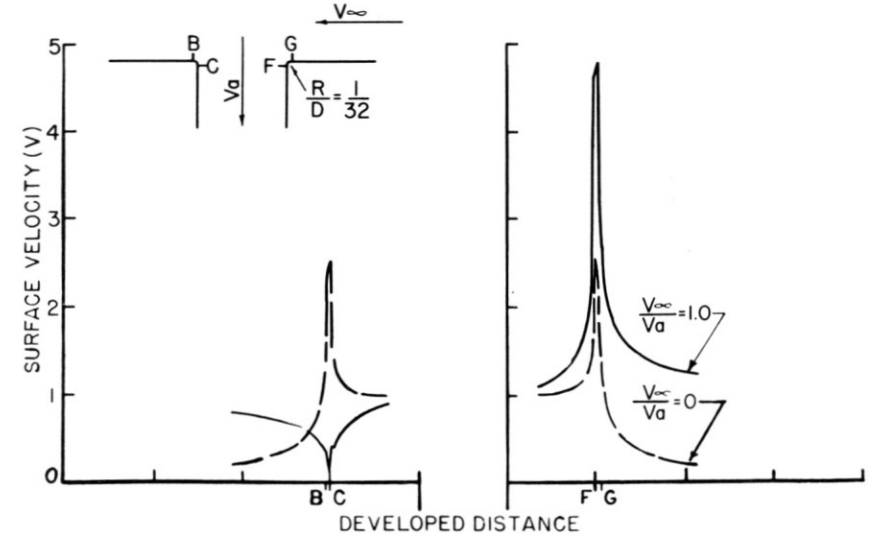

Figure 4*b*. Surface velocities ($R/D = 1/32$).

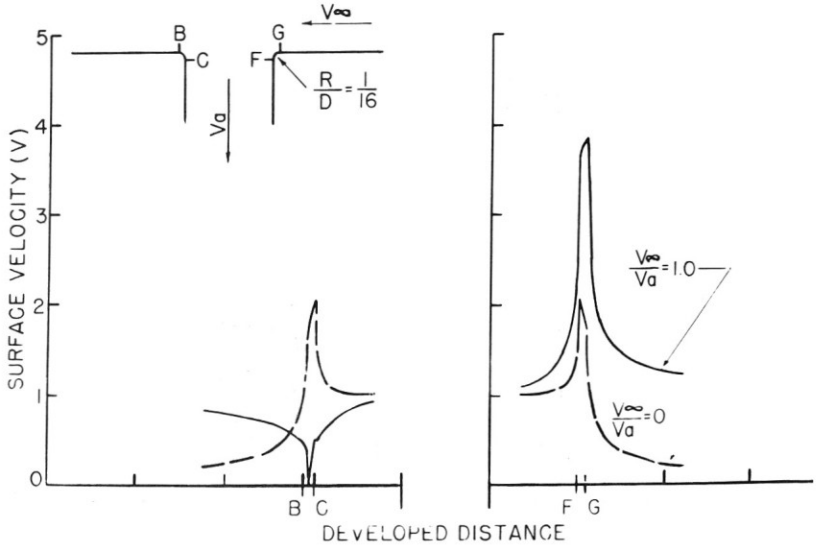

Figure 4*c*. Surface velocities ($R/D = 1/16$).

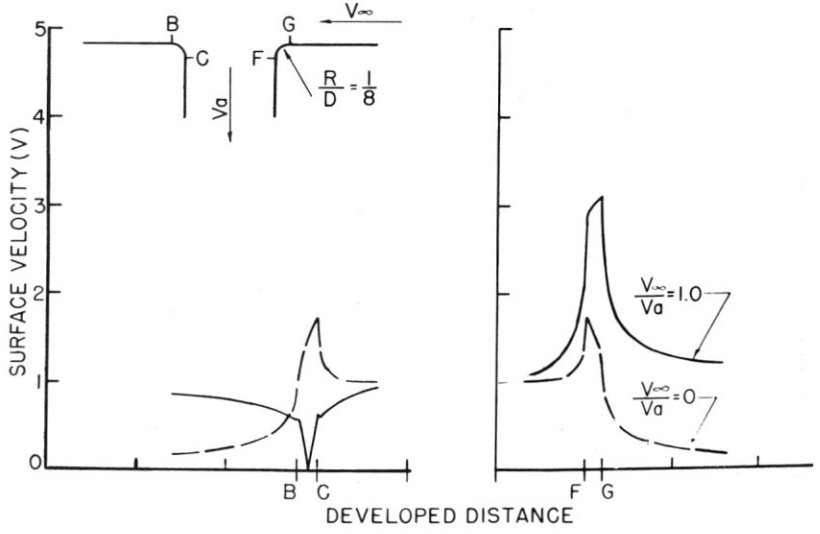

Figure 4*d*. Surface velocities ($R/D = 1/8$).

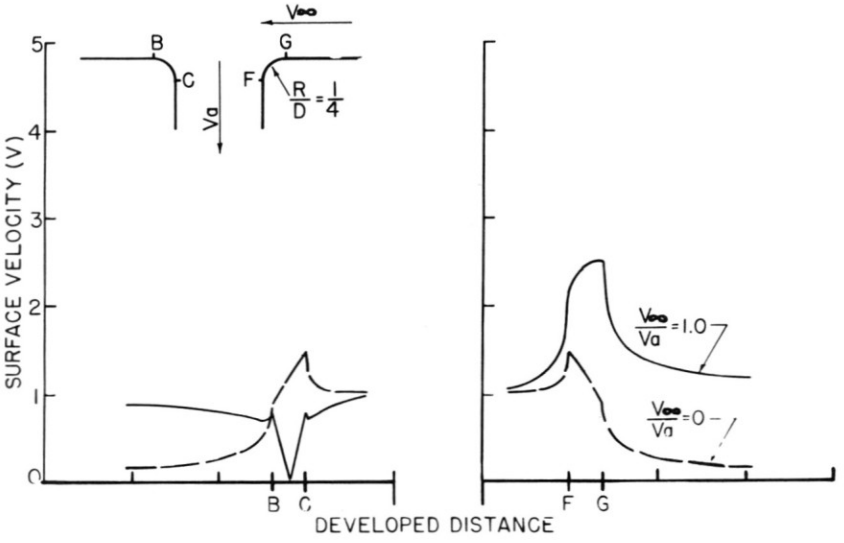

Figure 4*e*. Surface velocities ($R/D = 1/4$).

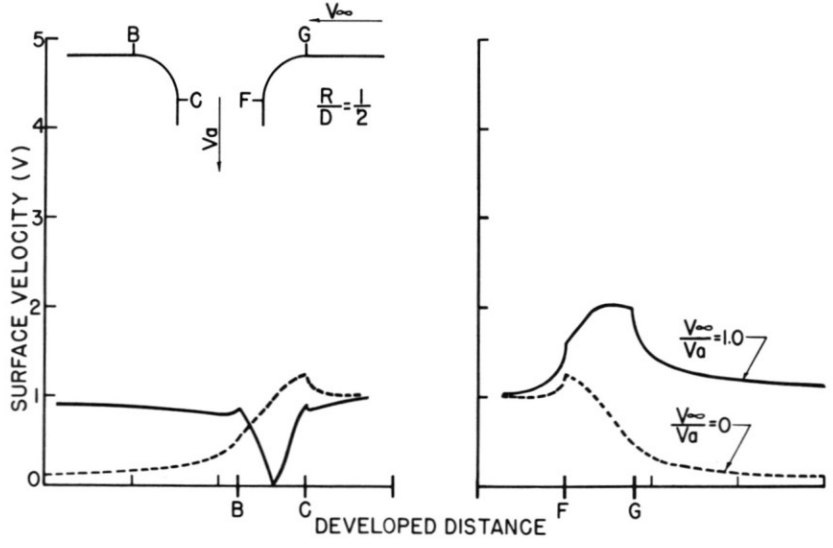

Figure 4*f*. Surface velocities ($R/D = 1/2$).

in the curved portion of the bellmouth, and last, a very sharp deceleration of the flow just at the end of the curved portion as the flow enters the parallel inlet passage. The velocity profiles on both sides of the inlet are identical because the cross flow is zero.

Examining now a cross-flow ratio of unity at the same R/D ratio of 1/8 the velocity peak on the upstream side is seen to be much higher (3.0 as opposed to 1.75 for no cross flow), and the decay to a velocity of 1.0 inside the duct is slower. On the downstream surface, the velocity drops to zero at the stagnation point, which occurs about half-way along the curved portion of the bellmouth, before rising towards unity well downstream of the bellmouth. Unwholesome cusps in the velocity curve are noted at the start and stop of the curved portion, arising presumably from the characteristics of the bellmouth contour as generated by the conformal transformation.

The effect of increasing the radius ratio is to decrease the severity of the velocity peaks, as is seen from the other portions of Fig. 4; the cusps in the profile are, however, evident even at the radius ratio of 1/2.

EXAMINATION OF NEAR-SURFACE VELOCITIES

The severity of the discontinuities in the slope of the velocity curves has prompted an investigation of velocities along streamlines close to the bounding surfaces. In Fig. 5, which examines conditions near the termination of the bellmouth, velocities along streamlines bounding ½ per cent

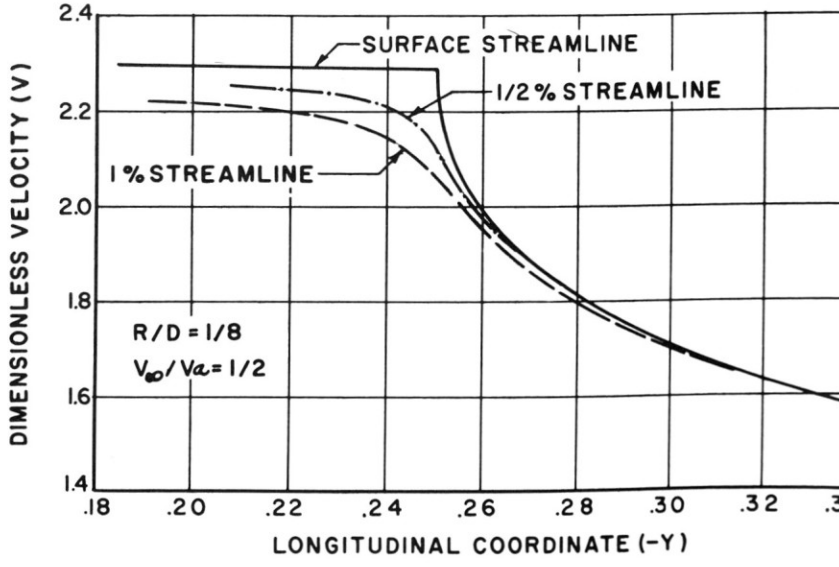

Figure 5. Near-surface velocity comparison.

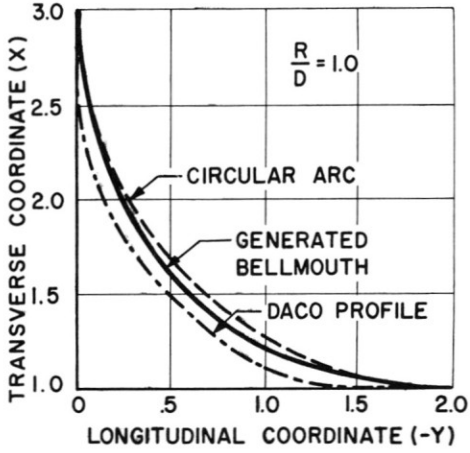

Figure 6*a*. Wall contour profile comparison (R/D = 1.0).

and 1 per cent of the total influx are plotted, along with the surface velocities. It is seen that the velocity gradients attenuate rapidly as one moves away from the surface.

Two inferences may be drawn from this observation. The first inference is that the effects of discontinuities in the second derivative are confined to the immediate area of the discontinuity, and hence that the main body of the flow field is unaffected by the small details of contour geometry. The second inference is that the coordinates of internal streamlines may be used to generate bellmouths with more attractive velocity gradients.

COMPARISON WITH OTHER CALCULATIONS

Comparable surface velocity data have been presented in an excellent paper by Smith of Douglas Aircraft Co. [1], wherein a distributed source technique is used. Smith's contour also approximates a circular arc, and is compared with that generated by the conformal transformation for a radius ratio of unity, in Fig. 6*a*. The surface velocity data are presented in Fig. 6*b*, where surface velocity is plotted as a function of developed distance for the pure-inflow case. The magnitude and location of the velocity peaks are very similar for the two methods; however, matching of the second derivatives at the points of tangency in the Smith study results in a rather smoother velocity curve.

CONCLUSIONS

1. The conformal transformation presented is believed to offer a quick, simple, and accurate solution for potential flow into a curved bellmouth.

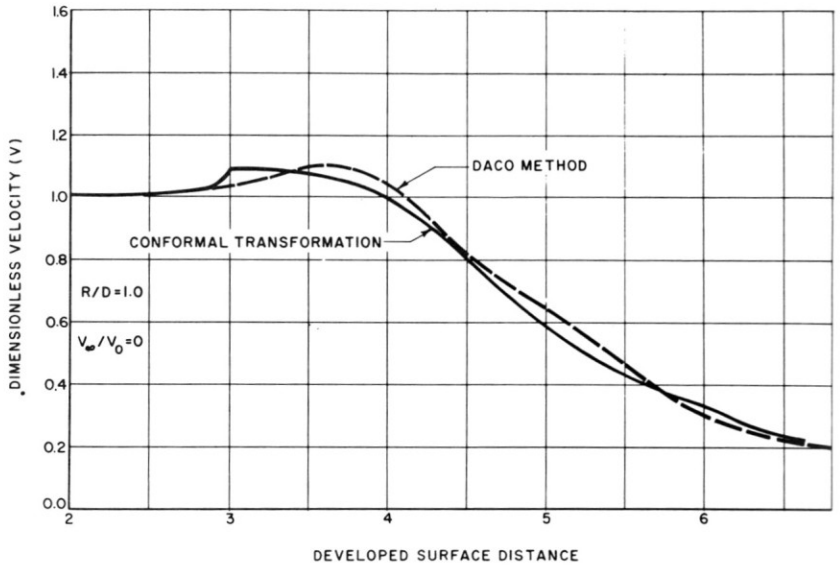

Figure 6*b*. Surface velocity comparison.

2. The surface contour generated by the transformation is not particularly desirable, in that discontinuities in the second derivatives of the contours generated lead to abrupt changes in pressure gradients. The effects of these surface deficiencies are, however, believed to be confined to the surface region.
3. From the point of view of achieving an even velocity distribution into a lifting fan, depth below the inlet surface is the most valuable geometric aid.
4. The effects of bellmouth geometry (i.e., radius ratio) are confined to an area immediately adjacent to the bellmouth, typically within one or two passage widths of the inlet.

REFERENCE

1. Smith, A. M. O., "Incompressible Flow about Bodies of Arbitrary Shape," IAS Paper No. 62-143 (Los Angeles, June 19–22, 1962).

ACKNOWLEDGEMENT

Special acknowledgement is made of the assistance provided in deriving and programming the transformation by K. L. Chandiramani, graduate student at the Massachusetts Institute of Technology, and summer employee at N.R.C. during 1962.

PART B. EXPERIMENTAL INVESTIGATION

ABSTRACT

The effects of cross flow on inlet performance are examined experimentally using a family of three simple inlets and four different inflow aids. Two inlets have a circular-arc lip contour and have lip radius ratios of 9 per cent and 25 per cent. The third inlet is asymmetrical with an elliptical arc leading lip and a small circular arc trailing lip. The aids are: a cambered closure plate, a cascade of inlet shutters, a trip fence and a perforated wall used for boundary-layer suction.

The inlet performance is analysed on the basis of surface pressure distributions at the symmetry plane and on average total pressure loss. All inlets except the shuttered one performed well under static inflow conditions. Under cross-flow conditions all three basic inlets showed evidence of strong adverse surface pressure gradients and suffered severely from flow separation.

INTRODUCTION

Presented here are the results of a recently completed wind tunnel programme. The programme is part of a continuing series of normal inlet studies. Whereas Part A was concerned with two-dimensional potential flow this part deals with real fluid flows into three-dimensional inlet models. The experimental work is closely tied to the fan-in-wing VTOL concept, but is valid also for more general normal inlet applications.

The inflow problem is distinctly twofold:

1. A problem of bulk flow nature: the core of the inflowing fluid behaves very much like the ideal fluid described in Part A. The velocity profile, on first entering, is highly nonuniform and distorted, particularly if cross flow is present. Its development is primarily a function of inflow distance and cross-flow ratio.
2. A problem of primarily surface flow nature: boundary-layer separation on the inlet surfaces is to be avoided.

The purpose of the experimental inlet studies is to investigate the performance of normal inlets under cross-flow conditions and, further, to test inflow aids suitable for relieving critical areas.

EXPERIMENTAL RIG AND INSTALLATION

TUNNEL FACILITY

The fan-in-wing inlet studies were made in the new N.R.C. VTOL propulsion wind tunnel which provides a low turbulence flow at up to 130 fps in a test section 10 ft $\times$ 20 ft (20 ft vertical dimension). Connections

to a large plant exhaust system permitted achievement of velocities up to 250 fps in the intakes tested.

INLET MODELS

The wind, into which the normal inlets were fitted, was an 80-in. chord airfoil of NACA 0015 section and had a 10-ft span. It was mounted on a suitably faired 24-in. diameter suction duct at the 10-ft level of the test section. It was possible to change the wing incidence through $\pm 12.5°$ by rotating the wing-duct assembly about a swivelling duct joint below the test section floor.

The inlets were of the annular type with outside and inside diameters of 24 in. and 12 in., respectively, and their axes were fixed at 35 per cent of the wing chord. The lip and centerbody top were faired in with the wing contour. The family of inlets tested had "simple" lip and centerbody contours, being either circular or elliptical arcs.

Three basic inlets were tested:

1.. $R/D = 9$ per cent inlet (R/D = lip radius to outside diameter ratio).
2. $R/D = 25$ per cent inlet.
3. An asymmetric inlet (elliptic leading lip and circular trailing lip).

The $R/D = 9$ per cent inlet was tested also with four different inflow aids (see Fig. 1). These were:

1. A closure plate cambered to fit the upper wing surface contour.
2. A cascade of fifteen inlet guide vanes immersed in the plane of the wing with individually adjustable vanes.
3. A perforated wall section located below the leading lip lower tangent point.
4. A 36-in.-long trip fence located near the leading edge of the wing and centered about the midspan.

The last two aids were used for boundary-layer-control experiments. The closure plate was examined to determine if it would function as a ramming device, deflecting air downward during forward flight.

INSTRUMENTATION

One semi-span of the wing, including the inlet and centerbody, was fully fitted out with surface static pressure taps. A fixed distance down in the inlet annulus (see Fig. 1) an eight-point rake using five-tube probe heads was employed to measure the inlet stream variables. The probes, while not calibrated individually, were manufactured with extreme care.

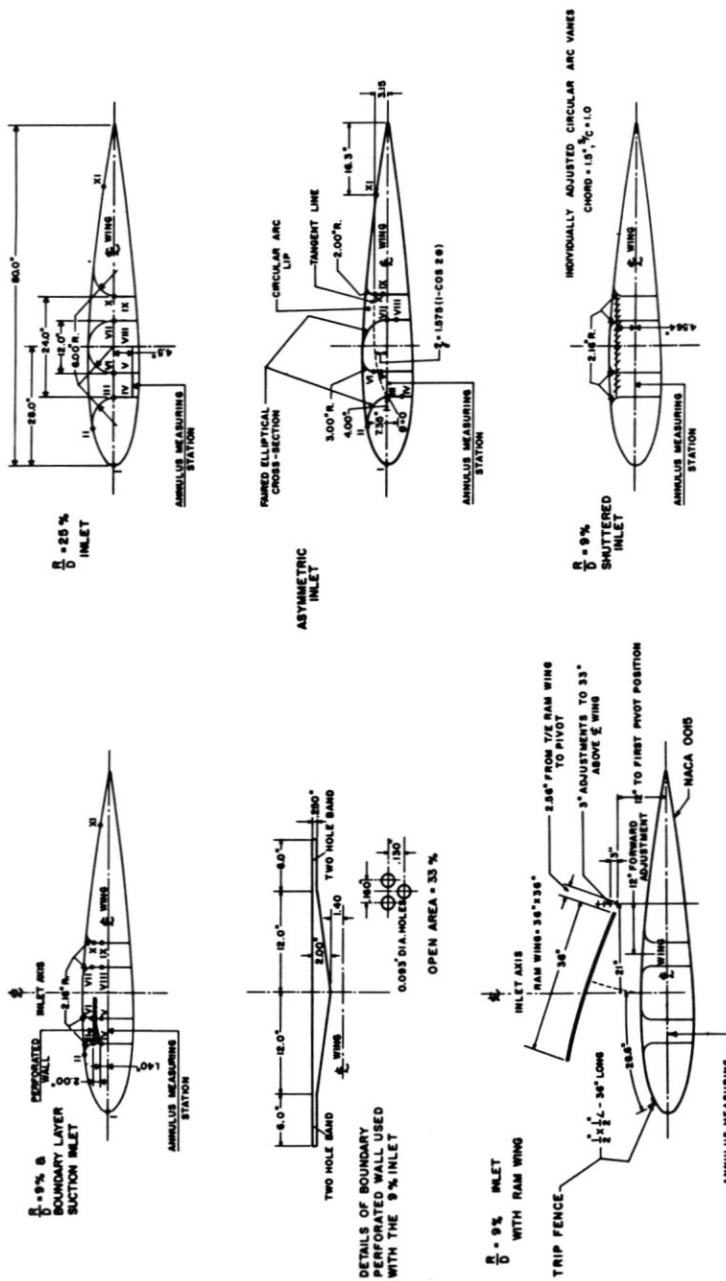

Figure 1. Wing inlet configurations.

A prototype probe head of like style was calibrated extensively [1] and its calibration data were applied to the measuring instruments. While the calibrated range of this probe includes velocity vector cone angles of up to 45°, the more accurate range extends only to 35°.

The suction inlet flow was set and monitored using a fixed array of Kiel type probes and wall static taps located in the vertical suction duct at about seven pipe diameters down from the inlet.

The cross flow (tunnel wind speed) was set and controlled by means of a Betz micromanometer, measuring the static pressure difference between the plenum chamber and working section.

TEST PROCEDURE

TUNNEL CALIBRATION AND CORRECTIONS

In order to evaluate the effect of the suction model on the tunnel velocity profile the test section was surveyed with a yawmeter rake at about one chord length upstream of the leading edge of the wing. The effect was observed to be quite small.

The tunnel's axial pressure distribution as measured by ceiling static taps showed that the suction model produced approximately the same blockage as the two-dimensional NACA 0015 wing, which was tested also in similar conditions in the same facility (note that in both cases the faired-in suction pipe was present.) The data published here, however, have not been corrected for tunnel interference. Some approximate corrections are given in the Appendix.

EXPERIMENTAL METHODS

The three basic inlets were subjected to the same test conditions, i.e., wing incidences of $-12.5°$, $0°$, $+12.5°$, and a nominal cross-flow ratio range of zero to 1.5. The inlet aids were tested in combination with the $R/D = 9$ per cent inlet and only under the more severe test conditions. The model test Reynolds number range was $2 \times 10^6 < \mathrm{Re} < 5.5 \times 10^6$, based on the 80-in. chord.

Inlet annulus pressure surveys were made for all tested configurations while surface pressure data were taken for all inlets except the shuttered one.

Only one side half of the inlet annulus was surveyed with the traversing gear. The inlet annulus pressure data were collected automatically giving a radial survey at each selected angular location. Angular increments of

15° and 30° were used. The sampling time per station was $3\frac{1}{2}$ minutes so that a complete survey, say at 30° increments, was completed in 24.5 minutes, neglecting indexing time. A total of 123 useful annulus surveys was made in the present testing programme.

Three inlet configurations required special optimization techniques and these are now discussed briefly.

R/D = 9 PER CENT INLET FITTED WITH CLOSURE (AND RAM) PLATE

Optimizing the plate's position and angle of attack relative to the wing was most important so as to maximize the plate's ramming capabilities. When used with the R/D = 9 per cent inlet the best position of the trailing edge of the plate (for all cross-flow ratios) was 12 in. above the chord line and 21 in. rearward of the inlet axis. The clearance thus provided allowed for good inlet flow under static inflow conditions as well as for shedding of the closure plate wake above the wing. The clearance should also be effective in providing an opening for the flyby of momentum separated foreign objects. Inlet tests were made with the plate fully raised (i.e., 57.5° relative to the wing) and repeated with the plate at an angle of attack at which its upper surface was at the point of stall.

R/D = 9 PER CENT INLET WITH SHUTTERS

Trial runs with both fixed and ganged movable vanes showed that the losses were unacceptably high. Consequently the vanes were adjusted individually for each test point. This procedure was complicated and it was impossible to avoid local vane stalls altogether, particularly at very low and very high cross-flow ratios. The test chord Reynolds number range for the vanes was $1.03 \times 10^5 < \mathrm{Re} < 2.16 \times 10^5$ and the Reynolds number effect is estimated to be small.

R/D = 9 PER CENT INLET WITH BOUNDARY-LAYER SUCTION

The unrepeatability of early test data obtained with the boundary-layer suction inlet prompted a close look at the possibilities of Reynolds-number effect on suction experiments. Tests were made holding one variable of the group V_∞ (tunnel velocity), m_a (inlet mass flow), m_b (bleed mass flow) constant at a time; no such effect was observed, but it may have been hidden by measuring uncertainties. Subsequently, the problem turned out to be one of very strong hysteresis phenomena involving boundary-layer stall and reattachment.

DATA REDUCTION PROCEDURES

The annulus probe data were handled by means of an IBM 1620 computer. The calibration data were entered for tabular lookup procedures and the raw five-tube pressure data were converted directly into swirl and radial (inflow) angles, static, total and dynamic pressures. From these values all other quantities such as velocity, mass flow, pressure loss, etc., and their averages were computed.

INLET PERFORMANCE

SURFACE PRESSURE DISTRIBUTION

In considering the boundary-layer development it is instructive to examine the surface-pressure distributions along the model symmetry plane, i.e., line I to XI; see Fig. 1. It is important to recall that all inlet contours here are either circular or elliptical arcs, and hence feature abrupt changes in curvature at the tangency points: II, IV, VI, VII, X, and at the top of the trailing lip. Figures 2 to 5 all show that strong negative and positive pressure gradients may exist on the inlet walls. The strongest positive pressure gradients were always found on the leading lip. Their second most common occurrence was at the rear of the centerbody. As the cross-flow ratio increased the suction peak on the leading lip grew and moved towards the upper tangent point (II). Separation started where the pressure gradient was most strongly positive and subsequently moved upstream.

The inflection of the pressure distribution curve between the leading edge and the leading lip (line I-II) is due to the superposition effect of the sink flow on the two-dimensional wing pressure distribution. The analytically predicted suction peaks are clearly visible, but occur farther upstream than predicted—in fact, nearer to the midlip position than III. It is quite probable that boundary-layer growth may be responsible for this difference.

In Figs. 2 to 4 only typical pressure distributions are shown for three cross-flow ratios: zero, maximum before boundary-layer stall, and a well-developed poststall.

R/D = 9 PER-CENT INLET

Examining the pressure data for the $R/D = 9$ per cent inlet it can be seen (Fig. 2) that at zero wing incidence boundary-layer separation occurs for $V_\infty/V_a > 0.25$, as indicated by the flatness of the pressure profile at III. For negative incidence of $-12.5°$ (i.e., forward tilt) separation is delayed

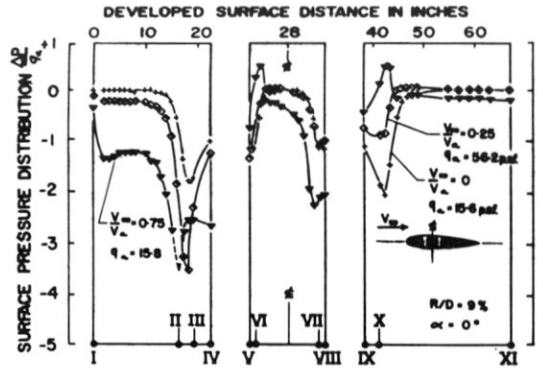

FIG. 2a ZERO WING INCIDENCE.

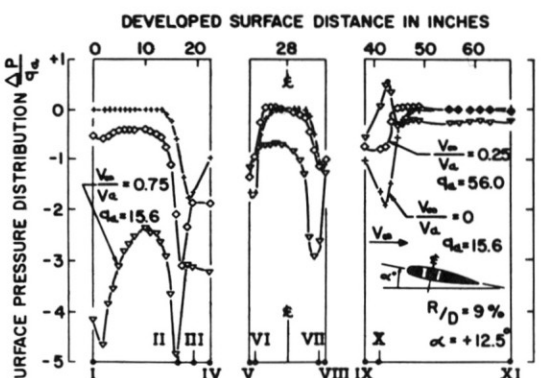

FIG. 2c POSITIVE WING INCIDENCE.

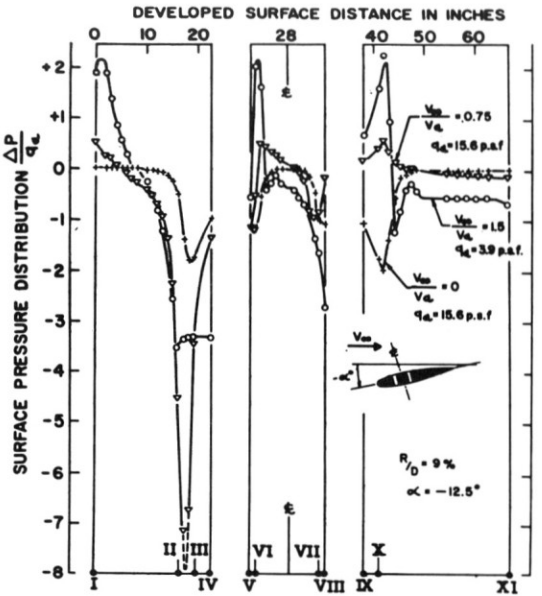

FIG. 2b NEGATIVE WING INCIDENCE.

Figure 2. Surface pressure distribution at the symmetry plane as a function of cross-flow ratio. $R/D = 9$ per cent inlet.

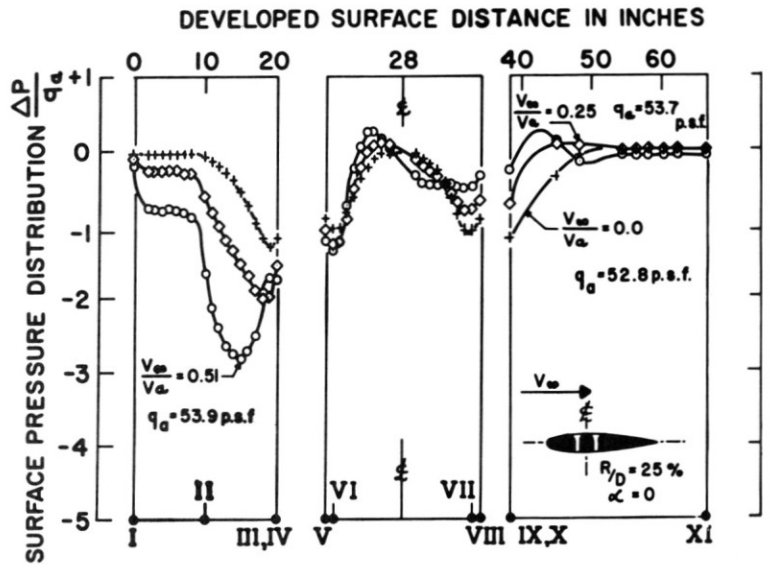

FIG.3a ZERO WING INCIDENCE.

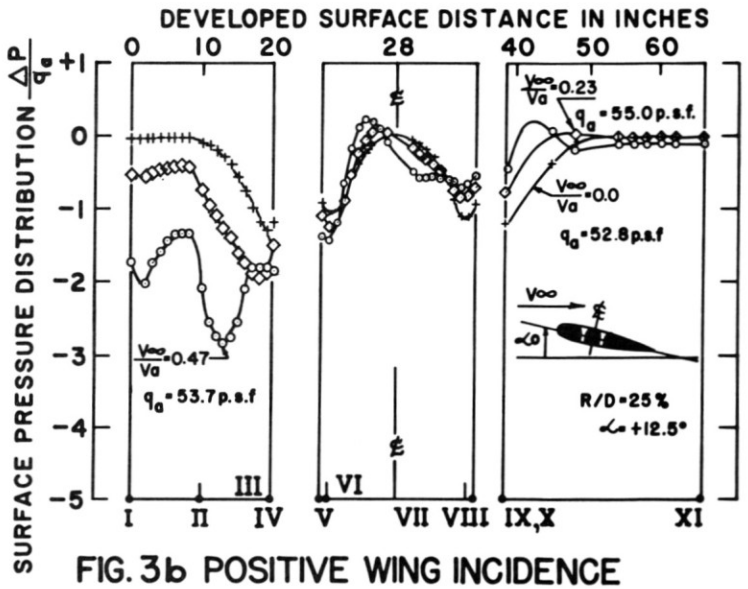

FIG. 3b POSITIVE WING INCIDENCE

Figure 3. Surface pressure distribution at the symmetry plane as a function of cross-flow ratio. $R/D = 25$ per cent inlet.

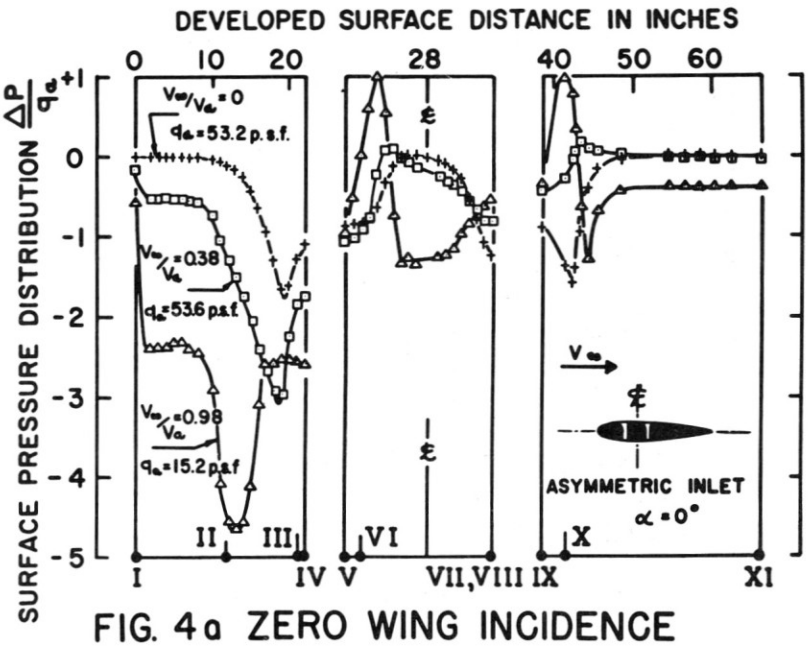

FIG. 4a ZERO WING INCIDENCE

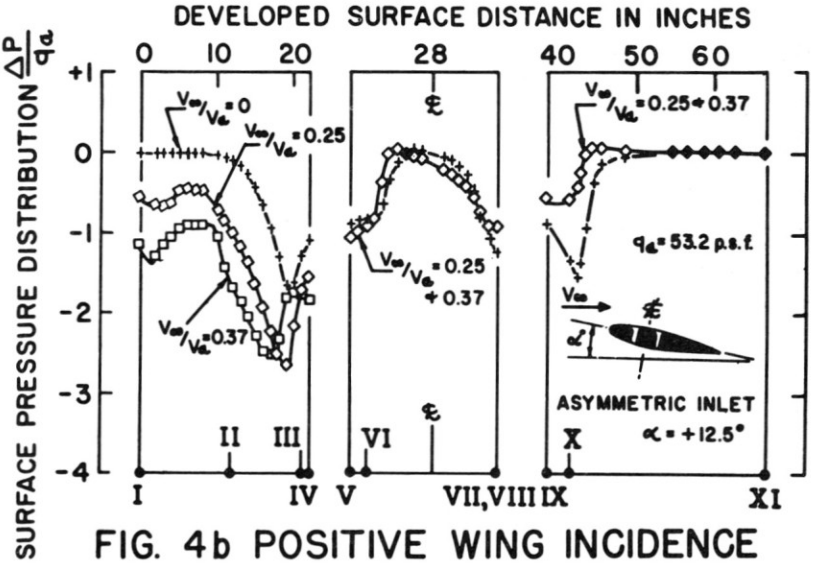

FIG. 4b POSITIVE WING INCIDENCE

Figure 4. Surface pressure distribution at the symmetry plane as a function of cross-flow ratio. Asymmetric inlet.

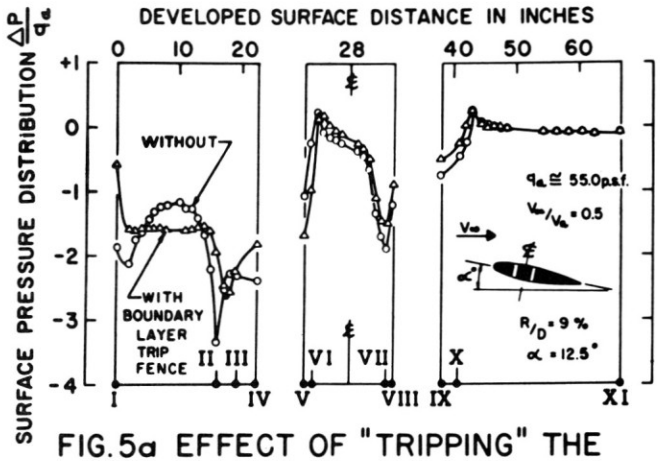

FIG. 5a EFFECT OF "TRIPPING" THE LEADING LIP BOUNDARY LAYER ON SURFACE PRESSURE DISTRIBUTION.

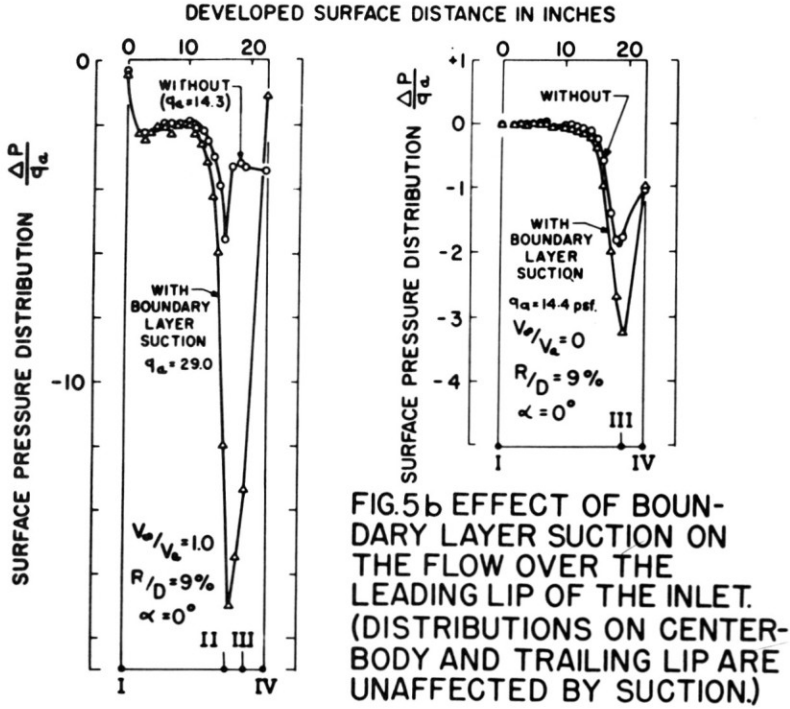

FIG. 5b EFFECT OF BOUNDARY LAYER SUCTION ON THE FLOW OVER THE LEADING LIP OF THE INLET. (DISTRIBUTIONS ON CENTER-BODY AND TRAILING LIP ARE UNAFFECTED BY SUCTION.)

Figure 5. Boundary-layer-control experiments pressure distributions.

until $V_\infty/V_a > 0.75$ while at positive incidence of $+12.5°$ it occurs at almost zero cross flow. These observations have been verified by inlet annulus data not shown here, and also by the total pressure-loss data shown in Fig. 7*a*. These ratios are considerably higher than reported on by Gregory [2] who, incidentally, used a real fan model. As is typical of stall phenomena generally, it is necessary to reduce the cross flow before the flow will reattach.

R/D = 25 PER CENT INLET

Referring to Fig. 3, it can be seen that at zero incidence leading lip separation occurs somewhere in excess of $V_\infty/V_a = 0.25$ (the actual value is $V_\infty/V_a = 0.37$), while at $+12.5°$ incidence the flow separates a little earlier, viz. at $V_\infty/V_a > 0.23$. In other words, increasing the lip radius appears to delay separation moderately. The pressure distributions on the trailing lip are not representative because the wall had an insufficient number of pressure taps; it is known that in the static case the pressure distribution all around the lip is relatively symmetrical, not as shown here. Concerning inlet distortion, it was observed that the inflow angles were generally a little greater for this inlet than noted for the previous one. This suggests that more inflow distance is required to straighten out the velocity profile before it becomes similar to the $R/D = 9$ per cent inlet profile.

ASYMMETRIC INLET

The inlet distributions shown in Fig. 4 demonstrate that, generally speaking, they resemble closely those of the $R/D = 25$ per cent inlet. The static pressure gradients over the centerbody certainly appear a little more favourable here than for any of the tested circular arc centerbodies.

TRIP FENCE INLET

Note the comparison of two distributions, one with and the other without the trip fence, as illustrated by Fig. 5*a*. The test conditions are similar: $V_\infty/V_a = 0.5$ and incidence angle $= +12.5°$. Tripping the boundary layer reduces the amount of surface velocity "peaking" and completely stops separation in this case. The distributions over the centerbody and trailing lip are virtually unchanged. Evidently, the initial conditions of the boundary layer are important to inlet performance. The trip fence forces the boundary layer, which is initially in the laminar-flow regime, to become turbulent. Once in a turbulent state the boundary layer can flow against a more strongly positive pressure gradient than it could while in a

laminar state. Annulus data not shown here showed that both the inlet angle and velocity distributions were much improved as well. The success of this simple experiment demonstrates clearly that inflow aids need not be complicated to be useful, and that much is to be gained by controlling the "effective" Reynolds number of the boundary layer.

BOUNDARY-LAYER SUCTION INLET

This second boundary-layer control experiment was even more impressive than the previous one. Again the pressure distribution is compared to the one of the $R/D = 9$ per cent inlet. (see Fig. 5*b*). With optimum bleed provided separation was completely averted for all test cross-flow ratio values at zero wing incidence. When adequate bleed was not maintained separation was immediate. The testing range was limited by the capacity of the bleed system. Figure 6 shows the necessary bleed requirement to keep the flow attached. It is instructive to observe that in-flight starting of a fan (tantamount to requiring the leading lip to reattach) consumes up to two times the bleed flow required to maintain flow already attached. This appears to be a very serious limitation to the practicable application of this inflow aid.

Annulus velocity data show that additional boundary-layer bleed may be necessary at the rear of the centerbody in order to attach local separation pockets at $\theta = 150°$. These separated flow regions have not been observed on the other inlets, probably because the leading lip always tended to separate first.

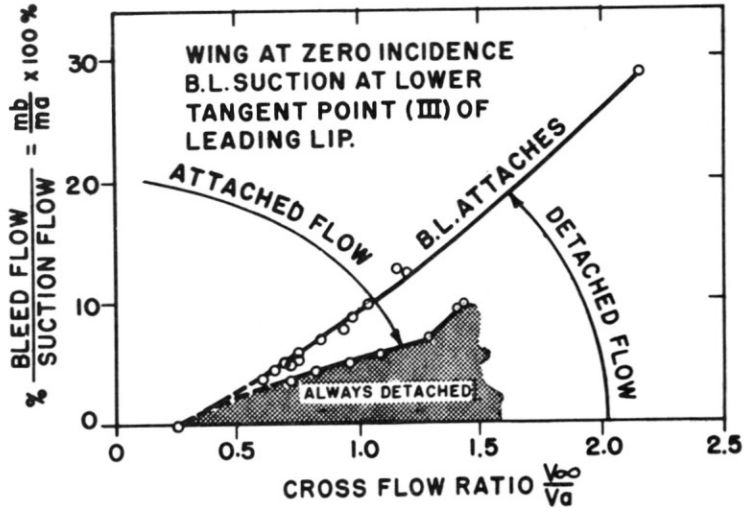

Figure 6. Boundary-layer bleed requirement.

TOTAL PRESSURE LOSS

The averages used here are based on measured mass flow, nominal annulus area, and the standard air density. Other more conventional averages were evaluated also, but were found to be influenced greatly by separated flow areas.

Thus

$$V_a' = \frac{m_a}{\rho_{\text{std}} A}$$

and

$$q_a' = \frac{m_a^2}{2g_0\rho_{\text{std}} A^2}$$

Hence total pressure loss (nondimensionalized) $= \Delta P_0/q_a'$

where

$$m_a = \sum \rho_i \Delta A_i \vec{V}_i$$

It is to be noted that none of the inlet measurements reflect boundary-layer losses within $\frac{1}{2}$ in. of the walls. Consequently, static tests for which the inlet boundary layer was estimated to be less than $\frac{1}{2}$-in. thick show virtually no total pressure loss. The inlet loss data have been conveniently assembled in Fig. 7. Because of the scarcity of data at large cross-flow ratios the discussion here is limited to the range $0 < V_\infty/V_a < 1.25$.

R/D = 9 PER CENT INLET

The inlet loss can be examined by means of Fig. 7*a*. At cross-flow ratios below 0.25 it is not possible to distinguish loss curve trends because differences are of the same order as the measuring uncertainties. It may be recalled, however, that the surface pressure data identified the separation point clearly. At cross-flow ratios in excess of 0.25 the losses increase continuously. It can be seen that only in the case of $-12.5°$ incidence does the loss become violent at separation. Except for the last case, the annulus data show a similar picture—gradual degeneration of the inlet profile throughout the whole annulus. Separated flows do not have sharp demarcation lines; they are bounded by wide regions of low velocity and with very large misalignment angles. For example: one inch away from the leading lip wall and 30° to the side of the symmetry plane for $V_\infty/V_a = 0.5$ at $\alpha = +12.5°$ the velocity is approximately $\frac{1}{5}$ of the local annulus

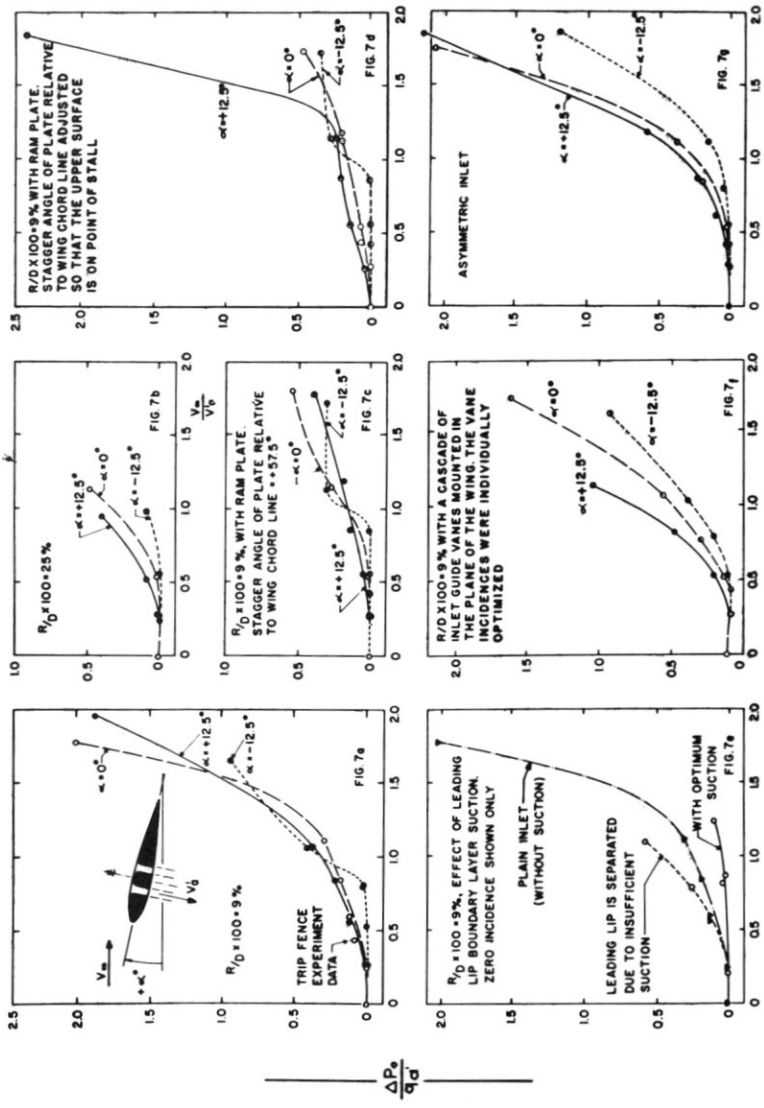

Figure 7. Total pressure loss as a function of cross-flow ratio.

maximum. The flow angles were: swirl greater than 43° (away from the leading lip) and about 20° for the radial plane angle (here the flow is radially outwards, so the flow is "overturning"). Away from the separated regions the flow is more axial where it is being deflected by the walls and least axial at the centerbody sides where the pressure gradient normal to the streaming direction has to effect turning unaided by the walls.

At negative wing incidence one might expect a more axial inflow distribution, and the experimental data bear this out. Up to cross-flow ratios of 1.0 the distribution remains more axial, but thereafter the distortion resembles more that of the zero and positive incidence tests.

R/D = 25 PER CENT INLET

The inlet loss data for the 25 per cent inlet are illustrated in Fig. 7*b*. The pressure loss at zero incidence is constant in the range $0 < V_\infty/V_a < 0.5$. At a positive wing incidence of +12.5° the loss exceeds very marginally that of the R/D = 9 per cent inlet. At −12.5° incidence both inlets feature similar losses in the cross-flow ratio range $0 < V_\infty/V_a < 0.8$. Leading lip stall is not discernible here and the flow appears to degenerate gradually. Since the R/D = 25 per cent inlet exhibits only marginal loss improvements over the R/D = 9 per cent inlet it seems highly undesirable from depth considerations to resort to large radius ratio inlets.

R/D = 9 PER CENT INLET FITTED WITH CLOSURE (AND RAM) PLATE

The loss performance of this configuration may be examined by means of Figs. 7*c* and 7*d*. The performance of the basic 9 per cent inlet is considerably improved at all test conditions except, perhaps, at low cross-flow ratios (and here some allowance should be made for uncertainty in measurement). At high cross-flow ratios the gains are particularly large.

Both loss and annulus data show that the inlet performance with the ram plate fully raised at +12.5° wing incidence is very similar to performance at zero wing incidence without ram plate aid. At zero wing incidence the plate delays separation and promotes flow reattachment for cross-flow ratios as high as 0.5.

In addition to reducing the total pressure loss the plate when fully raised helps greatly both in "straightening" the flow at the inlet plane for all test conditions and in obstructing least in the static (zero cross flow) case.

Evidently, when the drag penalty is of no concern, or is even beneficial (as, for instance, when starting a transition manoeuvre prior to landing), the best performance is achieved with the plate fully raised. This is when

the ram recovery is greatest and when the inlet momentum drag can be employed usefully for starting a stationary fan. On the other hand, during the takeoff transition, when drag is to be minimized, it may be profitable to have a programmed closure rate.

ASYMMETRIC INLET

The loss characteristics as seen in Fig. 7*g*, and also the pressure data of Fig. 4, show that the performance of the asymmetric inlet resembles closely that of the $R/D = 25$ per cent inlet. This seems a little surprising since the lip radius ratio at the lower tangent point is only 16 per cent—i.e., in between the two circular arc radius ratios tested. Looking back on this experiment and the potential flow studies, it is estimated that the performance might have been better had the major and minor axes of the elliptical arc been interchanged.

$R/D = 9$ PER CENT INLET WITH SHUTTERS

As can be seen from Fig. 7*f*, the vaned inlet is the least efficient of all inlets tested. The loss at zero cross flow is quite high because the vane chamber over the rear half of the inlet is "wrong." At all cross flows, in spite of very careful vane adjustment, severe corner stalls were observed at the vane pivot ends (the vanes did not touch the end walls). By far the worst separation (occurring at all cross-flow ratios tested) appeared at the rear of the centerbody where a vane was very near to the centerbody surface. There was no evidence that the vanes helped to keep the leading-lip boundary layer attached to the leading lip. Furthermore, the vanes were not effective in making the inflow more nearly axial.

$R/D = 9$ PER CENT INLET WITH BOUNDARY-LAYER SECTION

Referring to Fig. 7*e*, the lowest inlet loss is seen to be associated with the optimum boundary-layer suction case. Note that for insufficient bleed the loss exceeds that for the plain $R/D = 9$ per cent inlet. The additional loss, it is thought, is attributable to a spreading of the separated region because of leakage flows into and out of the perforated wall.

As the cross-flow ratio is increased while using continuous bleed on the leading lip, the flow eventually separates from the rear of the centerbody. The lowest cross-flow ratio for which such a separation was noted was $V_\infty/V_a = 0.75$ and its location was in the region $160° < \theta < 180°$, at both sides of the centerbody. The separated flow areas increased with cross-flow ratio with the result that at $V_\infty/V_a = 1.0$ the region extended from $\theta = 150°$ right around the rear of the centerbody. Again, the separated flows were bounded by the aforementioned low velocities and misalignment.

CONCLUSIONS

1. None of the three simple inlets tested gives satisfactory inlet flows under cross-flow conditions. Strong positive pressure gradients appear on the curved walls and cause the boundary layer to separate.
2. The $R/D = 9$ per cent inlet performs very efficiently under static inflow conditions.
3. The closure plate is an effective device for increasing the ram recovery of inlets. It seems especially well suited for in-flight starting of lifting fans.
4. The trip fence experiment demonstrates that flow separation on the leading lip may be delayed effectively by forcing the boundary layer to become turbulent before entering the inlet.
5. Boundary-layer suction can be used to prevent inlet separation, but the required relative mass flow to reattach separated flows is high.

REFERENCES

1. Schaub, U. W., C. R. Sharp, and R. W. Bassett, "An Investigation of the Three-dimensional Flow Characteristics of a Non-nulling Five-tube Probe," N.R.C. LR-393 (February 1964).
2. Gregory, M. A., W. G. Raymer, and Edna M. Love, "The Effect of Forward Speed on the Inlet Flow Distribution and Performance of a Lifting Fan Installed in a Wing," NPL Aero Rep. 1018, A.R.C. 23,839 (June 1962).

APPENDIX

Because the validity of correcting high-lift device data for tunnel interference is somewhat uncertain, the data here have not been corrected for tunnel constraints; but plausible corrections are set out below. The model size was, however, matched carefully to the test section size so as to minimize both scale and interference effects.

Using standard correction formulae the following interference coefficients have been estimated:

1. Horizontal interference coefficient [1A]. This coefficient is based on the plain wing (with the inlet covered) at zero incidence and is directly applicable to the cross-flow ratio. Horizontal interference coefficient $= (1 - \epsilon) = 1.08$

$$\therefore V_\infty \text{ corrected} = V_\infty \text{ measured} \times 1.08$$

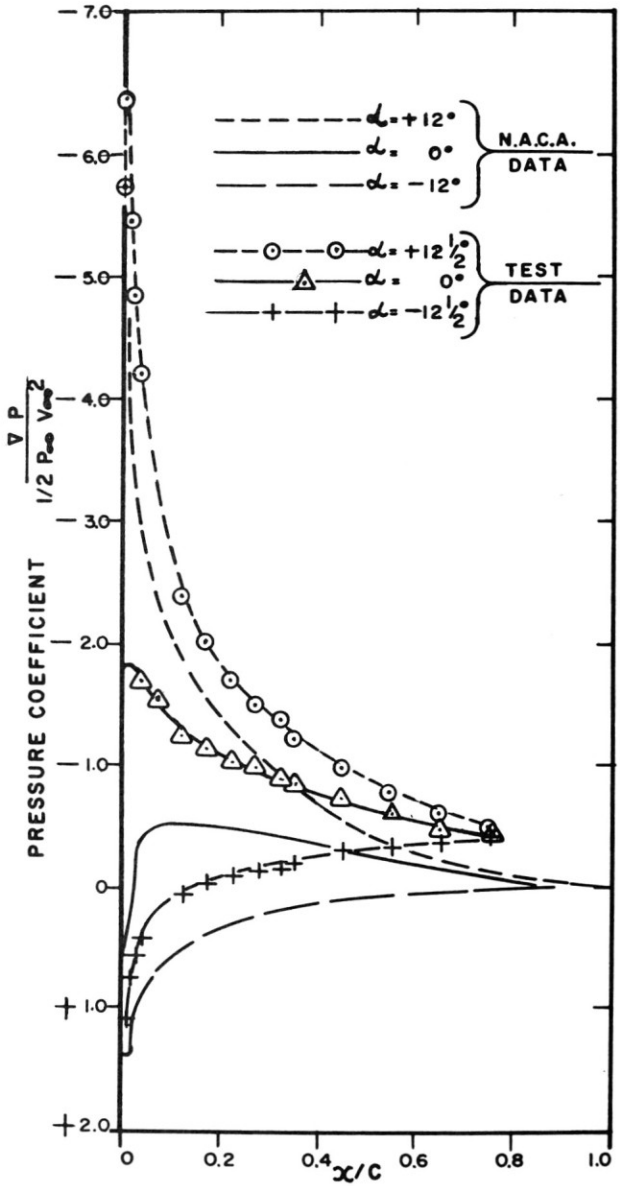

Figure A1. Comparison between the corrected pressure distribution of an N.A.C.A. 0015 section and the uncorrected pressure distribution of the test model with covered inlet.

2. Incidence and camber angle correction coefficients [1A]. These values have been derived using NACA 0015 lift and pitching moment coefficients.

   Geometric incidence angle = $\pm 12.5°$
   Incidence angle correction = $+0.2°$
   Camber angle correction = $+0.2°$

   For conventional models the maximum incidence angle correction due to wall interferences should be less than 2° [2A], and this is clearly achieved.

3. "Jet" boundary (or duct) correction factors [3A]. The nonuniformity of the interference velocity due to the efflux jet boundary (or the duct in this case) should be no greater than 2 to 5 per cent for detailed pressure measurements in the inlet annulus. The absolute magnitudes actually estimated are:

Incidence angle	+12.5	0	−12.5
$\Delta V_a/V_a$ (per cent)	−1.15	−1.51	−1.8

A good qualitative comparison between the uncorrected surface pressure distribution of the wing model (with the inlet covered in and mounted on the duct) and the standard (free air) NACA pressure distribution on the NACA 0015 section [4A] can be made by examining Fig. A1.

REFERENCES

1A. Pankhurst, R. C., and D. W. Holder, *Wind Tunnel Technique* (London; Pitman, 1952).

2A. Anscombe, A., and J. Williams, "Some Comments on High-Lift Testing in Wind Tunnels with Particular Reference to Jet-Blowing Models, "Rep. 63, AGARD, North Atlantic Treaty Organization, Paris (August 1956).

3A. Heyson, Harry H., "Jet Boundary Corrections for Lifting Rotors Centered in Rectangular Wind Tunnels," NASA TR R-71.

4A. Graham, Donald J., Gerald E. Nitzberg, and Robert N. Olson, "A Systematic Investigation of Pressure Distributions at High Speeds over Five Representative NACA Low-Drag and Conventional Airfoil Sections," NACA Report No. 832 (1945).